Accepted Manuscript

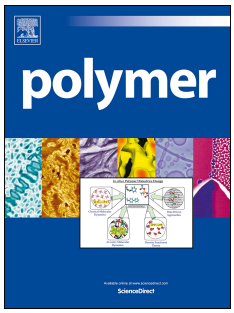

Anchor installation on porous polymer networks (PPNs) for high CO_2 uptake

Xinyu Yang, Lanfang Zou, Hong-Cai Zhou

PII: S0032-3861(17)30687-0

DOI: 10.1016/j.polymer.2017.07.028

Reference: JPOL 19840

To appear in: *Polymer*

Received Date: 10 January 2017

Revised Date: 29 June 2017

Accepted Date: 9 July 2017

Please cite this article as: Yang X, Zou L, Zhou H-C, Anchor installation on porous polymer networks (PPNs) for high CO_2 uptake, *Polymer* (2017), doi: 10.1016/j.polymer.2017.07.028.

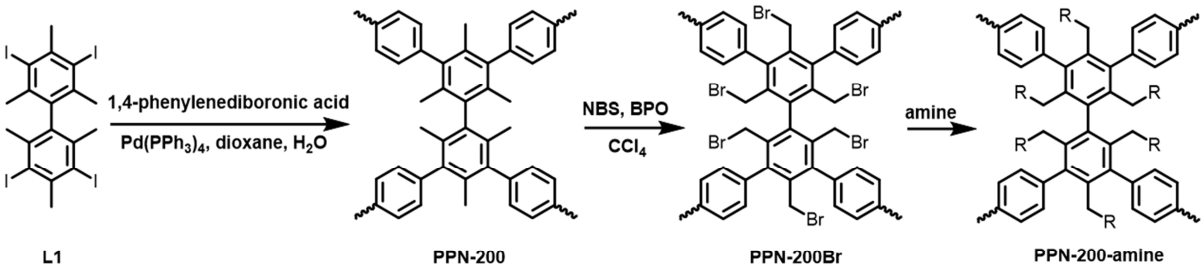

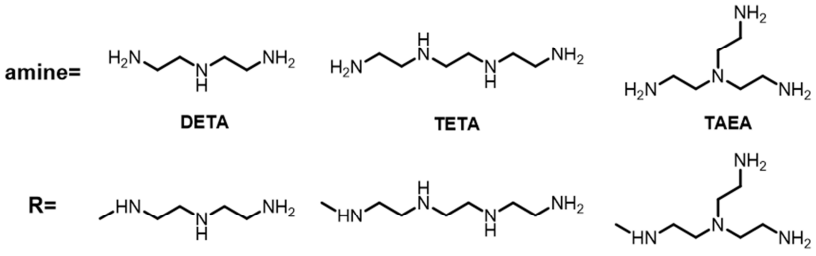

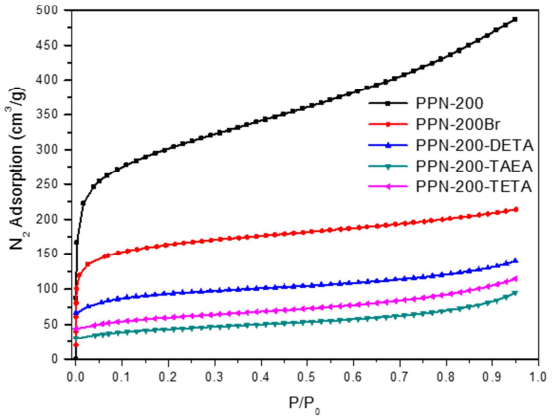

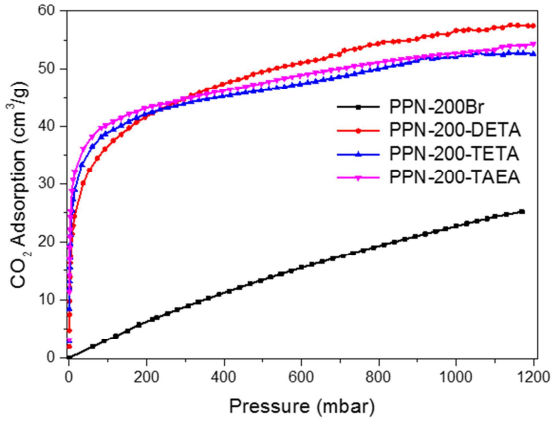

Anchor Installation on Porous Polymer Networks (PPNs) for High CO_2 Uptake

Xinyu Yang,[a] Lanfang Zou,[a] Hong-Cai Zhou[a, b, *]

[a] Department of Chemistry, Texas A&M University, College Station, Texas 77843-3255, United States

[b] Department of Materials Science and Engineering, Texas A&M University, College Station, Texas 77842, United States

X.Y and L.Z contributed equally to this work

Corresponding author: zhou@chem.tamu.edu

Abstract

Porous polymer networks (PPNs) is an emerging category of advanced porous materials that are of interest for carbon capture due to their high physicochemical stability and convenient functionalization process. Herein, a series of alkylamine tethered PPN-200 (PPN-200-DETA, PPN-200-TETA and PPN-200-TAEA) were prepared through a novel post-synthetic strategy. Due to the presence of alkylamine groups, PPN-200-TAEA has CO_2 uptakes of 42 cm^3/g (at 298 K and 150 mbar) and 55 cm^3/g (at 298 K and 1 bar), and a calculated CO_2/N_2 selectivity of 289, which demonstrate its potential in postcombustion carbon capture application.

1. Introduction

With the rapid increase of the global population and the industrialization, the consumption of energy is growing explosively. Currently over 85% of the global energy demand is being supported by fossil fuels, which will continue to play an important role in the foreseeable future.(1-4) The burning of the fossil fuels releases large amounts of CO_2 into the atmosphere, which has made the CO_2 concentration in the atmosphere increase from 280 ppm to 390 ppm since the beginning of the industrial age.(5-8) The increase of the CO_2 concentration affects the incoming and outgoing energy in the atmosphere, resulting in an increase of the average atmospheric temperature. Though researchers are exploring cleaner forms of energy (such as solar energy and hydrogen) (9-11) to replace the fossil fuels, these are far from practical application. Subsequently, strategies for carbon capture and sequestration (CCS) are urgently required.(12, 13) In real applications, the combustion of fossil fuels in air generates flue gas consisting of a majority of N_2 with 15% CO_2 and other minor components such as H_2O, CO, NO_x and SO_x; thus, CO_2-uptake capacity at about 0.15 bar is more relevant to realistic postcombustion applications. Aqueous alkanolamines, such as monoethanolamine (MEA) solutions, have been utilized as postcombustion “wet scrubbing” methods in power plants due to their large CO_2 capacity and selectivity. However, this method suffers from many complications, such as high regeneration energy, toxicity and the corrosive nature of amines.

As an alternative choice, the solid porous materials are very promising for CCS since they can overcome the downsides of aqueous alkanolamine solutions. During the past decades, metal−organic frameworks (MOFs) have been studied extensively due to their high surface area, tunable pore size, adjustable functionalities and the potential in gas adsorption and separation.(14-16) Even though some MOFs with high densities of open metal sites (Mg-MOF-74) or high amounts of amine loading (mmen-MOF-74) have shown high CO_2 uptakes, the practical application of most MOFs is limited by their poor physicochemical stability and, particularly, by sensitivity to water.(17-19)

PPNs are another class of very promising candidate materials for carbon capture, which are constructed from rigid monomers through covalent bonds and possess permanent porosity.(20-25) Due to their covalent connections, PPNs normally display exceptional chemical and water stability, enabling them to be easily functionalized by pre-synthetic or post-synthetic methods.(20-23) The introduction of alkylamines into PPNs can significantly enhance the CO_2 adsorption and CO_2/N_2 selectivity by utilizing the polarizability and quadrupole moment of CO_2, which have been demonstrated by Zhou and co-workers.(20) Nevertheless, till now, there are few works that present novel methods of introducing alkylamines into PPNs.

Herein, a novel post-synthetic strategy was designed to construct a series of alkylamine tethered PPNs, which demonstrated high carbon capture capability and CO_2/N_2 selectivity. First, PPN-200 was synthesized by Suzuki-Miyaura cross-coupling reaction using L1 and 1,4-phenylenediboronic acid. The default diamondoid framework topology (**dia** topology) constructed by the combination of tetrahedral unit and linear unit provides widely open and interconnected pores to efficiently eliminate the "dead space". More importantly, the extremely robust scaffold of PPN-200 makes it an ideal platform for introducing CO_2-philic groups under harsh reaction conditions. By reaction with N-bromosuccinimide (NBS), PPN-200 was modified to give PPN-200Br. The methylbromide groups can be further substituted by alkylamines (diethylenetriamine (DETA), triethylenetetramine (TETA) and tris(2-aminoethyl)amine (TAEA)) to produce PPN-200-amines (PPN-200-DETA, PPN-200-TETA and PPN-200-TAEA) (Scheme 1). The resulting alkylamine tethered PPN-200s showed significant increases in CO_2 uptake capacities (~55 cm^3/g at 298 K and 1 bar) and high CO_2/N_2 selectivity (289).

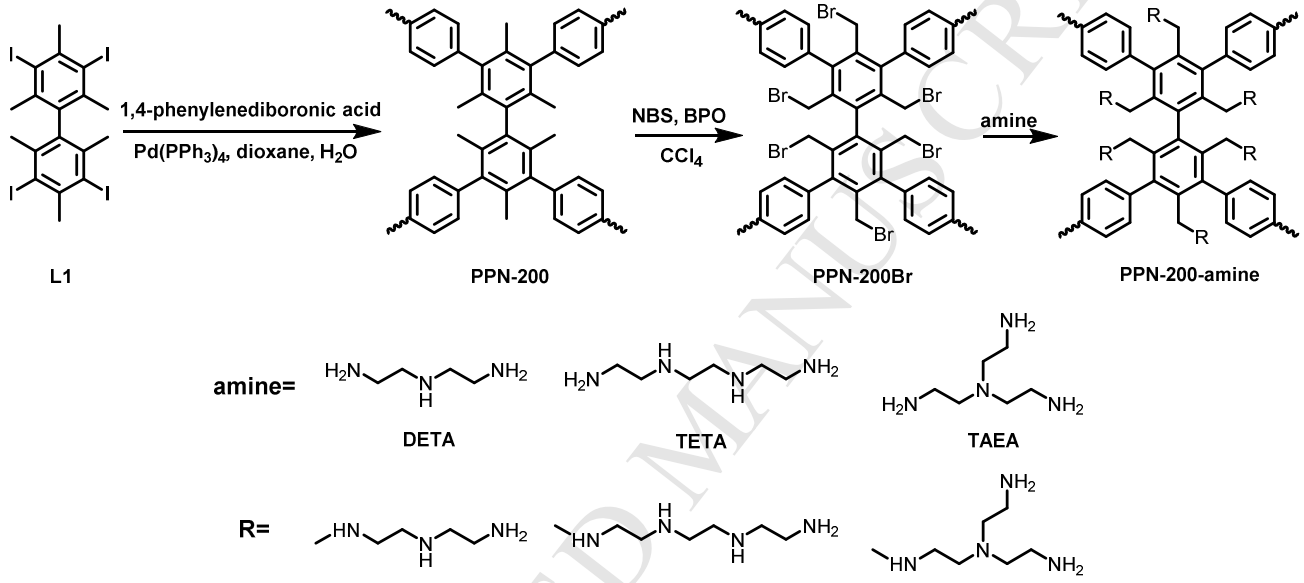

Scheme 1. The synthetic route of PPN-200amines.

2. Experimental

2.1 Materials

All chemicals were purchased from Sigma-Aldrich or Acros Organics and were used as received without further purification.

2.2 Instruments

Fourier transform infrared measurements (FT-IR) were performed on a SHIMADZU IR Affinity-1 spectrometer. Nuclear magnetic resonance (NMR) data were collected on a Mercury 300 spectrometer. N_2 and CO_2 adsorption–desorption isotherms were measured using a Micromeritics ASAP 2020 system at different temperatures. Powder X-ray diffraction (PXRD) was performed with a BRUKER D8-Focus Bragg–Brentano X-ray powder diffractometer equipped with a Cu sealed tube (λ = 1.54178 Å) at 40 kV and 40 mA. Thermogravimetric analysis (TGA) was conducted on a TGA-50 (SHIMADZU) thermogravimetric analyzer from room temperature to 600 °C at a ramp rate of 5 °C/min in a flowing nitrogen atmosphere. Scanning electron microscope (SEM) was performed on QUANTA 450 FEG and energy dispersive X-ray spectroscopy (EDS) was carried out by X-Max20 with Oxford EDS system equipped with X-ray mapping

2.3 *Synthesis of **2,2',4,4',6,6'-hexamethylbiphenyl***

To a 1000 mL three-necked flask containing 7.0 g of magnesium pieces, degassed anhydrous tetrahydrofuran (THF, 600 mL) and a pinch of iodine were added under a nitrogen atmosphere. The resulting mixture was

heated to 80 °C, and then 2-bromomesitylene (35 mL) was added dropwise. The reaction mixture was refluxed for another 3h. After it was cooled down to room temperature, a mixture of anhydrous $FeCl_3$ (1.1 g), 1, 2-dibromoethane (12 mL) and anhydrous THF (15 mL) was added under a nitrogen atmosphere. Stirring was continued for another 1 h, and then the reaction was quenched by the addition of hydrochloric acid. Organic solvents were evaporated under reduced pressure. The residue was extracted with dichloromethane. The dichloromethane phase was dried over anhydrous $MgSO_4$ and filtered. Most of dichloromethane was removed under reduced pressure, and then methanol was added. 2,2',4,4',6,6'-hexamethylbiphenyl was collected as white solid. (8.5 g, 31% yield). ^{1}H NMR (300 MHz, $CDCl_3$) δ: 6.93 (s, 4H), 2.33 (s, 6H), 1.86 (s, 12H).

2.4 *Synthesis of* ***3,3',5,5'-tetraiodo-2,2',4,4',6,6'-hexamethylbiphenyl (L1)***

To a mixture of 2,2',4,4',6,6'-hexamethylbiphenyl (4.0 g), solid iodine (7.0 g) and H_5IO_6 (3.1 g) in a 500 mL flask, $CH_3COOH/H_2O/H_2SO_4$ was added (240/48/7.2 mL). The resulting mixture was stirred at 90°C for 3 days. The reaction mixture was diluted with large amount of water. The precipitate was filtered and washed with water. The pink solid was collected and dissolved in $CHCl_3$, then washed with a saturated $Na_2S_2O_3$ solution to remove iodine residue. The organic phase was dried over anhydrous $MgSO_4$, filtered and evaporated under reduced pressure to produce 3,3',5,5'-tetraiodo-2,2',4,4',6,6'-hexamethylbiphenyl as a white solid (10.6 g, 85% yield). ^{1}H NMR (300 MHz, $CDCl_3$) δ: 2.05 (s, 12 H), 3.02 (s, 6 H).

2.5 *Synthesis of* ***PPN-200***

3,3',5,5'-tetraiodo-2,2',4,4',6,6'-hexamethylbiphenyl (148.2 mg), 1,4-phenylenediboronic acid (66.4 mg), CsF (1.216g) and $Pd(PPh_3)_4$ (20mg) were charged in a three-necked round bottom flask, followed by three evacuation and refill cycles with nitrogen on a Schleck line. A 20 ml degassed mixture of dioxane/water (9:1 in volume) was added to the reaction flask through a cannula. The mixture was stirred at 100 °C under a N_2 atmosphere for 48 h. After cooling to room temperature, the mixture was filtered and the solid was washed with DMF (30 ml × 3), methanol (30 ml × 3), H_2O (30 ml × 3), acetone (30 ml × 3) and dried in vacuo to obtain PPN-200 (71.4 mg, yield 92.4%) as pale yellow solid.

2.6 *Synthesis of* ***PPN-200Br***

PPN-200 (280 mg), N-bromosuccinimide (NBS) (0.852 g) and benzoyl peroxide (BPO) (100 mg) were combined in anhydrous CCl_4 (150 ml), and the mixture was refluxed for 48 h. After cooling to room temperature, the mixture was filtered, and the solid was washed with DMF, methanol, H_2O and acetone and dried in vacuo to obtain PPN-200Br (380 mg, yield 28%).

2.7 *Synthesis of* ***PPN-200-amines***

PPN-200Br (80 mg) in 20 ml amine (DETA/TETA/TAEA) was heated to 90℃ for 72 h. The resulting solid was centrifuged and washed with DMF (30 ml × 3), methanol (30 ml × 3), H_2O (30 ml × 3), acetone (30 ml × 3) and then dried in vacuo to afford the final product. (PPN-200-DETA, yield 85%; PPN-200-TETA, yield 81%; PPN-200-TAEA, yield 96%)

3. Results and discussion

A high surface area is critical for PPN-200 to investigate its properties and is also essential for postsynthetic modification. So we first optimized the synthetic conditions of PPN-200 by a series of control experiments (Figures 1a-1c, Table S1). The first series of experiments were designed to determine an appropriate solvent system. We chose different ratios of dioxane and water as solvents, ranging from 20:0, 18:2, 16:4, 14:6, 12:8 to 10:10. As shown in Figure 1a, to obtain a porous polymer, it was essential to utilize a mixture of dioxane and water. If pure dioxane was used, we only observed nonporous polymers, whose N_2 adsorption was very close to 0, due to the poor solubility of base in dioxane. But, if too much water was used, the decreasing solubility of L1 in the mixed solvent led to the decreased N_2 adsorption of PPN-200, which peaked at the ratio of 18:2. After determining a suitable solvent, the next step was to optimize the type and amount of base. From the Figure 1b and Figure 1c, we can see

that the porosities of PPN-200 synthesized by using CsF were much higher than those with K_2CO_3. With the increase of the amount of CsF, the N_2 adsorption of PPN-200 increased and peaked at 10 equivalents; after that, the N_2 adsorption decreased as more CsF was used (Figure 1c).

By combining best synthetic conditions, we determined the PPN-200 with highest N_2 adsorption (486 m^3/g) under 1 bar with an adsorption/desorption hysteresis loop (Figure 1d). Its Langmuir surface area, Brunauer-Emmett-Teller (BET) surface area, and pore volume are 1483 m^2/g, 944 m^2/g, and 0.48 cm^3/g, respectively. Its pore size distribution was calculated by the Density Functional Theory (DFT) method (Figure 2b). Its pore diameters are widely distributed from 10 Å to more than 60 Å, and no pattern could be identified from the pore size distribution plot, which implies the amorphous nature of PPN-200. This can also be confirmed by powder X-ray diffraction (PXRD) pattern (Figure S1) and scanning electron microscope (SEM) (Figures S8-S12). The most prominent pores have diameters of 11 Å and 14 Å, which is consistent with the microporous nature of PPN-200.

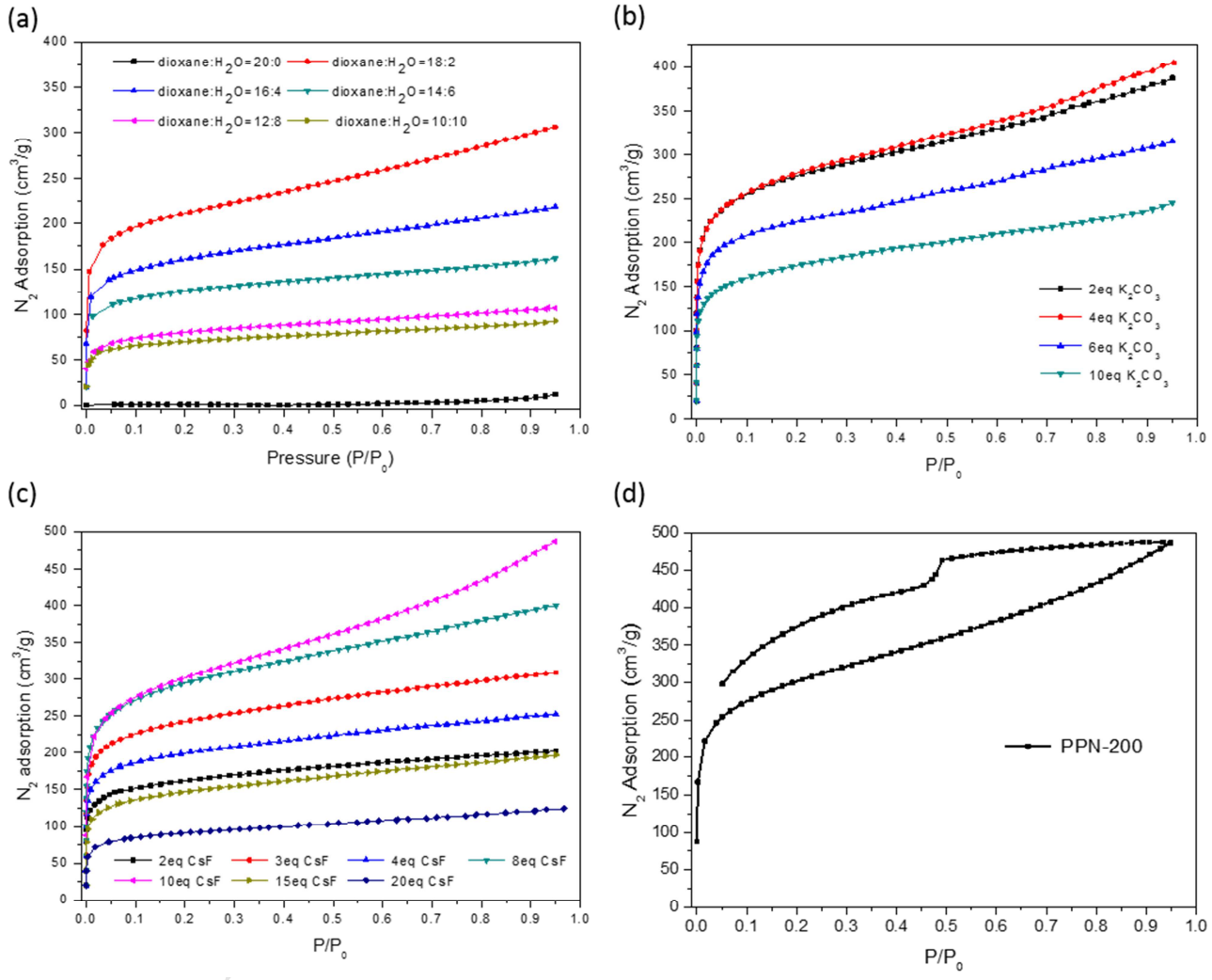

Figure 1. N_2 sorption at 77 K with changing solvent (a), different amount of K_2CO_3 (b) and CsF (c), (d) N_2 isotherm of optimized PPN-200.

After acquiring the highly porous PPN-200, we brominated it by using NBS to form the active intermediate PPN-200Br, which followed by substitution with excess alkylamines to yield PPN-200-amines (PPN-200-DETA, PPN-200-TETA and PPN-200-TAEA). The PPN-200Br and PPN-200-amines showed dramatic decreases in N_2 uptake (Figure 2a), which confirm that the functionalization occurs within the cavities. The occurrence of amine substitution was confirmed by TGA (Figures S3-S7), EDS (Table S2) and infrared spectroscopy (IR) (Figure S2),

from which we can clearly find there was a broad peak (from 3100 to 3500 cm^{-1}) belonging to alkylamines. The introduction of amine groups into PPN-200 resulted in materials with excellent CO_2 adsorption at 298 K and low pressures (Figure 2c). The trend of improvement in CO_2 adsorption under low pressure (0.15 bar) in terms of tethered amine groups was TAEA > TETA > DETA. Though the PPN-200-TAEA has the lowest N_2 adsorption, it presents the highest CO_2 adsorption of all amine-tethered PPN-200s, which indicates the CO_2 uptake capacity is closely related to the amount of amine instead of the surface area. PPN-200-TAEA exhibits high CO_2 adsorption: 42 cm^3/g (8.3 wt%) at 298 K and 0.15 bar and 55 cm^3/g (10.9 wt%) at 298 K and 1 bar. The CO_2/N_2 selectivity of PPN-200-TAEA in flue gas conditions was evaluated by the ratio of the adsorbed gas quantity where the partial pressure for CO_2 is 0.15 bar and N_2 is 0.85 bar. The calculated single-component CO_2/N_2 selectivity of PPN-200-TAEA in flue gas at 298 K is 289 that is significantly larger than other N-riched PPNs.

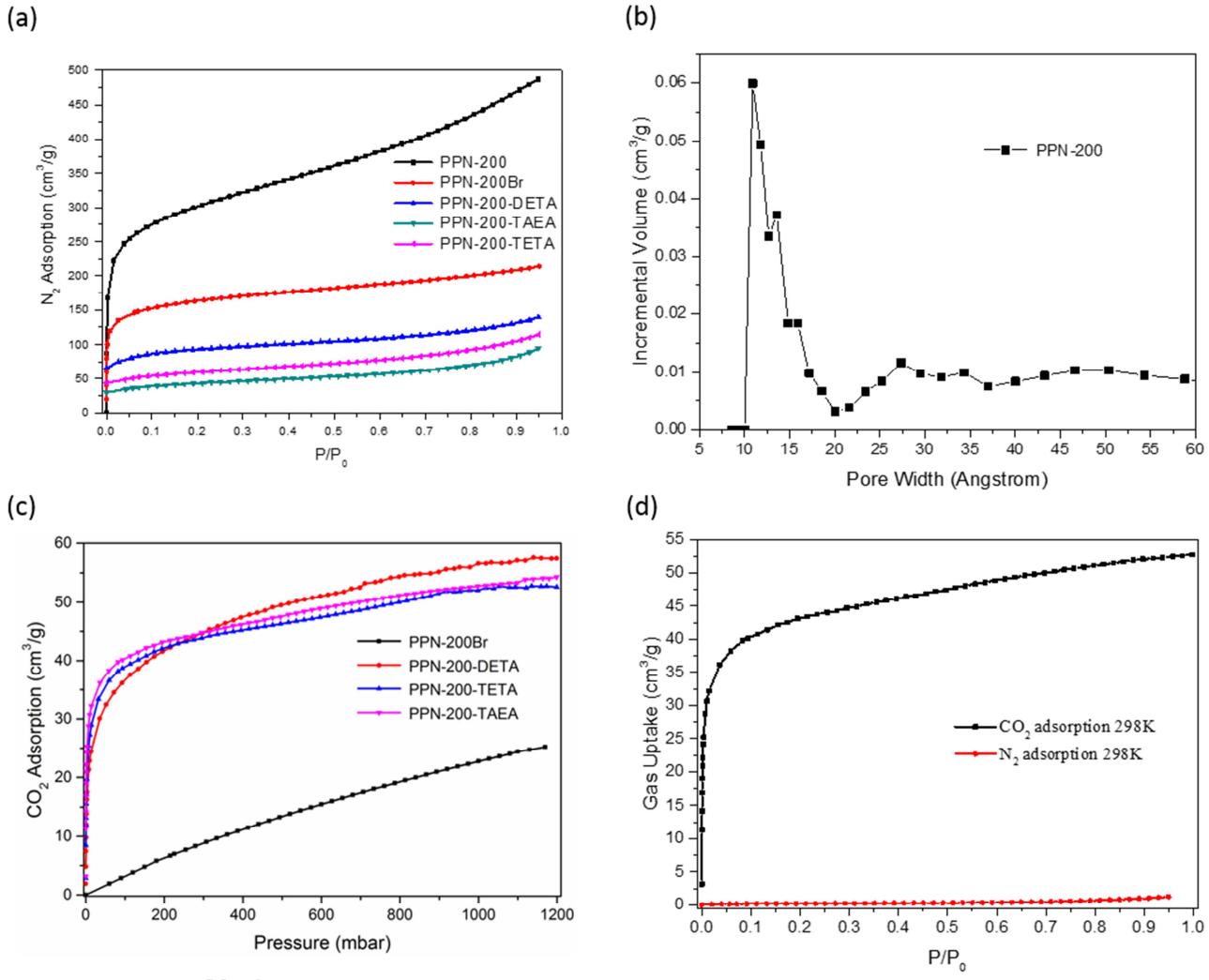

Figure 2. (a) N_2 isotherms of PPN-200, PPN-200Br, and PPN-200-amines, (b) pore size distribution of PPN-200, and (c) CO_2 adsorption of PPN-200Br and PPN-200-amines, (d) CO_2 and N_2 adsorption for PPN-200-TAEA at 298K.

4. Conclusion

In conclusion, we have successfully designed a novel strategy to synthesize a series of alkylamine functionalized PPN materials (PPN-200-DETA, PPN-200-TETA, and PPN-200-TAEA), which demonstrated excellent carbon capture properties. Among them, the CO_2 uptake of PPN-200-TAEA reaches 42 cm^3/g (8.3 wt%) at 298 K and 0.15 bar and its calculated CO_2/N_2 selectivity reaches 289. Given the outstanding physicochemical stability and high

CO_2 adsorption amount under 0.15 bar, the PPN-200-TAEA has great potential for practical application in postcombustion carbon capture.

5. Acknowledgements

This work was supported by U.S. Department of Energy Office of Fossil Energy, National Energy Technology Laboratory (DE-FE0026472) and as part of the Center for Gas Separations Relevant to Clean Energy Technologies, an Energy Frontier Research Center funded by the U.S. Department of Energy, Office of Science, Basic Energy Sciences under Award Number DE-SC0001015. The authors gratefully acknowledge Mr. Jeremy Willman for proofreading.

6. Reference

[1]. Caldeira K, Wickett ME. Oceanography: Anthropogenic carbon and ocean pH. Nature. 2003;425(6956):365-.

[2]. Hurst JK. In Pursuit of Water Oxidation Catalysts for Solar Fuel Production. Science. 2010;328(5976):315-6.

[3]. Korre A, Nie Z, Durucan S. Life cycle modelling of fossil fuel power generation with post-combustion CO_2 capture. International Journal of Greenhouse Gas Control. 2010;4(2):289-300.

[4]. McGlade C, Ekins P. The geographical distribution of fossil fuels unused when limiting global warming to 2 ^oC. Nature. 2015;517(7533):187-90.

[5]. Friedlingstein P, Andrew RM, Rogelj J, Peters GP, Canadell JG, Knutti R, et al. Persistent growth of CO_2 emissions and implications for reaching climate targets. Nature Geosci. 2014;7(10):709-15.

[6]. Frolicher TL, Winton M, Sarmiento JL. Continued global warming after CO_2 emissions stoppage. Nature Clim Change. 2014;4(1):40-4.

[7]. Jenkinson DS, Adams DE, Wild A. Model estimates of CO_2 emissions from soil in response to global warming. Nature. 1991;351(6324):304-6.

[8]. Parrenin F, Masson-Delmotte V, Köhler P, Raynaud D, Paillard D, Schwander J, et al. Synchronous Change of Atmospheric CO_2 and Antarctic Temperature During the Last Deglacial Warming. Science. 2013;339(6123):1060-3.

[9]. Abdin Z, Alim MA, Saidur R, Islam MR, Rashmi W, Mekhilef S, et al. Solar energy harvesting with the application of nanotechnology. Renewable and Sustainable Energy Reviews. 2013;26:837-52.

[10]. Grätzel M. Solar Energy Conversion by Dye-Sensitized Photovoltaic Cells. Inorganic Chemistry. 2005;44(20):6841-51.

[11]. Guo CX, Guai GH, Li CM. Graphene Based Materials: Enhancing Solar Energy Harvesting. Adv. Energy Mater. 2011;1(3):448-52.

[12]. Scott V, Gilfillan S, Markusson N, Chalmers H, Haszeldine RS. Last chance for carbon capture and storage. Nature Clim Change. 2013;3(2):105-11.

[13]. Wall T, Stanger R, Liu Y. Gas cleaning challenges for coal-fired oxy-fuel technology with carbon capture and storage. Fuel. 2013;108:85-90.

[14]. McDonald TM, Lee WR, Mason JA, Wiers BM, Hong CS, Long JR. Capture of Carbon Dioxide from Air and Flue Gas in the Alkylamine-Appended Metal–Organic Framework mmen-Mg2(dobpdc). J. Am. Chem. Soc. 2012;134(16):7056-65.

[15]. Simmons JM, Wu H, Zhou W, Yildirim T. Carbon capture in metal-organic frameworks-a comparative study. Energy & Environ. Sci. 2011;4(6):2177-85.

[16]. Sumida K, Horike S, Kaye SS, Herm ZR, Queen WL, Brown CM, et al. Hydrogen storage and carbon dioxide capture in an iron-based sodalite-type metal-organic framework (Fe-BTT) discovered via high-throughput methods. Chem. Sci. 2010;1(2):184-91.

[17]. Banerjee R, Phan A, Wang B, Knobler C, Furukawa H, O'Keeffe M, et al. High-Throughput Synthesis of Zeolitic Imidazolate Frameworks and Application to CO_2 Capture. Science. 2008;319(5865):939-43.

[18]. Phan A, Doonan CJ, Uribe-Romo FJ, Knobler CB, O'Keeffe M, Yaghi OM. Synthesis, Structure, and Carbon

Dioxide Capture Properties of Zeolitic Imidazolate Frameworks. Acc. Chem. Res. 2010;43(1):58-67.

[19]. Wang B, Cote AP, Furukawa H, O/'Keeffe M, Yaghi OM. Colossal cages in zeolitic imidazolate frameworks as selective carbon dioxide reservoirs. Nature. 2008;453(7192):207-11.

[20]. Lu W, Sculley JP, Yuan D, Krishna R, Wei Z, Zhou H-C. Polyamine-Tethered Porous Polymer Networks for Carbon Dioxide Capture from Flue Gas. Angew. Chem. Int. Edit. 2012;51(30):7480-4.

[21]. Rabbani MG, Reich TE, Kassab RM, Jackson KT, El-Kaderi HM. High CO2 uptake and selectivity by triptycene-derived benzimidazole-linked polymers. Chem. Comm. 2012;48(8):1141-3.

[22]. Rabbani MG, Sekizkardes AK, El-Kadri OM, Kaafarani BR, El-Kaderi HM. Pyrene-directed growth of nanoporous benzimidazole-linked nanofibers and their application to selective CO2 capture and separation. J. Mater. Chem. 2012;22(48):25409-17.

[23]. Zhang M, Perry Z, Park J, Zhou H-C. Stable benzimidazole-incorporated porous polymer network for carbon capture with high efficiency and low cost. Poly. 2014;55(1):335-9.

[24]. Dawson R, Adams D, Cooper A. Chemical tuming of CO2 sorption in robust nanoporous organic polymers. Chem. Sci., 2011, 2, 1173

[25]. Dawson R, Stevens L, Drage T, Snape C, Smith M, Adams D, Cooper A. Impact of water coadsorption for carbon dioxide capture in microporous polymer sorbents. J. Am. Chem. Soc. 2012, 134, 10741-10744

In this paper, a novel post-synthetic strategy was designed to construct a series of alkylamine tethered PPNs (PPN-200-DETA, PPN-200-TETA, and PPN-200-TAEA), which demonstrated excellent carbon capture properties. Among them, the CO_2 uptake of PPN-200-TAEA reaches 42 cm^3/g (8.3 wt%) and its calculated CO_2/N_2 selectivity reaches 289. Given the outstanding physicochemical stability and high CO_2 adsorption under 150 mbar, the PPN-200-TAEA has great potential for practical application in a post-combustion CO_2 capture.